Article

Multi-Objective Optimization of Plate-Fin Heat Exchangers via Non-Dominated Sequencing Genetic Algorithm (NSGA-II)

Shengchen Li [1], **Zixin Deng** [1], **Jian Liu** [1] **and Defu Liu** [1,2,*]

1   College of Mechanical and Electrical Engineering, Central South University, Changsha 410083, China
2   State Key Laboratory of High Performance Complex Manufacturing, Changsha 410083, China
*   Correspondence: liudefu@csu.edu.cn; Tel.: +86-731-88879351

Abstract: The rules of heat transfer and fluid flow in plate-fin heat exchanger are intricate and complex, and the selection of boundary conditions is the key to giving full play to the performance of heat exchanger. In this paper, a multi-objective optimization based on computational fluid dynamics (CFD) and non-dominated sequencing genetic algorithm (NSGA-II) was carried out to obtain the optimal performance of a plate-fin heat exchanger for an extended-range hybrid vehicle engine. The angle of serrated staggered fin, oil flow rate, and water flow rate were taken as input parameters, and the heat transfer quantity, oil pressure drop, and oil outlet temperature were taken as objective functions to perform the optimization analysis of the heat exchanger. Support vector machine regression (SVR) was used to establish the objective function, and the NSGA-II algorithm was adopted to obtain the Pareto optimal solution set. The optimal solution was determined in the Pareto optimal solution set by comprehensive evaluation based on technique for order preference by similarity to an ideal solution (TOPSIS). The results showed that the best comprehensive performance of the heat exchanger was achieved at a fin angle of $63.01°$, an oil flow rate of 9.7 L/min, and a water flow rate of 6.45 L/min. At this time, the heat transfer quantity was 9.79 kW, the oil pressure drop was 13.63 kPa, and the oil outlet temperature was 65.11 °C.

Keywords: plate-fin heat exchanger; serrated staggered fins; heat transfer; NSGA-II; multi-objective optimization

1. Introduction

Plate-fin heat exchangers are widely used for heat dissipation in automotive engines because of their compact and lightweight structure, good heat transfer performance, and low production cost [1]. Serrated staggered fins are common enhanced heat exchange surfaces in plate-fin heat exchangers. The principle is that the fins are periodically staggered at certain intervals from each other along the fluid flow direction, so that the boundary layer formed by the fluid near the fin surface enters the rear row of fins before it fully develops, making full use of the boundary layer separation effect. At the same time, the tail vortexes generated by the fluid on the upstream fins also have an excitation and enhancement effect on the heat transfer of the downstream fins [2,3]. In recent years, with the improvement of engine performance requirements of the extended-range hybrid vehicle engine, the requirements of the heat exchanger have been gradually increased, and many scholars have attempted to introduce new algorithms for heat exchanger optimization design research. At present, new algorithms, such as the genetic algorithm [4], annealing simulation algorithm [5], and model search algorithm [6], have been successfully applied to heat exchanger optimization design research [7]. However, these optimization algorithms have rarely been applied in engineering practice, and there is a lack of computational procedures for heat exchanger optimization design which can guide engineering application. At the same time, there is little research on plate-fin heat exchangers, which are widely used for automotive engine heat dissipation. Therefore, it is of great interest to conduct optimization design research and program development for plate-fin heat exchangers.

The optimal design of heat exchangers using traditional methods such as the logarithmic mean temperature difference (LMTD) method and the Efficiency-number of Heat-transfer Units (η-NTU) method is costly and time-consuming [8]. With the rapid development of computational fluid dynamics (CFD) and computer technology, it has become possible to use computers to optimize the design of heat exchangers with high efficiency. Studies by many researchers have shown that simulations of various types of heat exchangers using CFD are reliable [9–12]. Therefore, CFD numerical simulations can minimize unnecessary tooling production costs, test work, and R&D time, and provide great convenience for efficient optimal design of heat exchangers.

Juan et al. [13] analyzed the effects of structural parameters on thermal characteristics of transverse direction (TD) type serrated fin by numerical simulation methods and found that the vortexes generated near the TD fin region enhanced the turbulence intensity to reduce the thickness of boundary and improve the synergy between the velocity and temperature gradient. Minsung et al. [14] used numerical simulation methods to investigate the aerothermal performance of a slanted-pin fin heat exchanger under high-speed-bypass stream condition, and found that the design of slanted-pin fin can make the heat exchanger lighter and smaller. However, in order to obtain the heat transfer and flow resistance characteristics of the heat exchanger as a whole, it is necessary to conduct numerical simulation analysis of the whole heat exchanger. Nevertheless, the fin scale is very small relative to the overall heat exchanger scale, and it is extremely inefficient to directly simulate numerically heat exchangers with complex structures, such as plate-fin type without the necessary simplifications. At present, porous media model is the most applied simplification method, which was first proposed by Patankar et al. [15] for the simulation of steam generators. Zhang et al. [16] studied the flow and heat transfer characteristics in finned-tube heat exchangers based on the porous media method, and analyzed the effect of air flow on the resistance characteristics and heat transfer performance, and the simulation results were verified by the measured data. Therefore, the simplification of the overall heat exchanger using the porous media method will help to achieve an efficient numerical simulation analysis of heat exchangers with complex structures, such as the plate-fin type.

Generally, numerical simulation results need to be combined with optimization algorithms to obtain the optimal solution. Many scholars have made many efforts to this end [17–19]. The non-dominated sequencing genetic algorithm (NSGA-II) is widely used for optimization design due to its advantages such as fast operation and good convergence of the solution set. Alireza et al. [20] adopted CFD and NSGA-II to carry out multi-objective optimization designs for the combustion chamber of CO steam boiler, and studied the multi-objective optimization problem with two input parameters and two objectives. Jing et al. [21] used numerical simulation method and NSGA-II for a multi-objective optimization of mini U-channel cold plate with SiO_2 nanofluid to obtain the optimal performance. However, the Pareto frontier obtained by NSGA-II is an optimal solution set, and these studies ultimately use subjective analysis to select the optimal solution from the Pareto solution set. Technique for order preference by similarity to an ideal solution (TOPSIS) can effectively avoid the subjectivity of data, and can well depict the comprehensive impact of multiple impact indicators [22]. Aminu et al. [23] comprehensively evaluated the Pareto optimal solution set of NSGA-II using TOPSIS and obtained the optimal performance of concentrated Photovoltaic-Thermoelectric hybrid system.

In this study, in order to obtain the optimal performance of the plate-fin heat exchanger, the fin angle of the heat exchanger and the inlet flow rate are optimally designed. Firstly, a fluid-solid coupling model of the heat exchanger is established based on commercial CFD software Fluent, and the serrated staggered fins are simplified using porous media. By changing the fin angle, oil flow rate and water flow rate, 45 numerical simulation test cases are designed. Additionally, based on the numerical simulation results, support vector machine regression (SVR) is used to establish regression models of heat exchanger performance (heat transfer, oil pressure drop, and oil outlet temperature) with respect to fin angle and inlet flow rate, and these regression models are also taken as the optimized

objective functions. Then, the Pareto optimal solution set of the objective function is obtained using NSGA-II. Finally, the optimal solution that leads to the best performance of the heat exchanger is preferred by the TOPSIS comprehensive evaluation method.

2. Numerical Simulation Modeling of Plate-Fin Heat Exchanger

2.1. Physical Model

The heat exchanger consists of 14 layers of fins as a whole. There are 1 to 14 layers from the bottom to the top, respectively. Among them, the odd layers are water-side fins, and the even layers are oil-side fins, and the water-side fins and the oil-side fins are arranged alternately, as shown in Figure 1. To simplify the mesh, a simplified three-dimensional model of the heat exchanger is established as shown in Figure 1b without affecting the simulation results, and the inlets and outlets of the oil and water sides are extended to eliminate the effect of outlet effects on the simulation results.
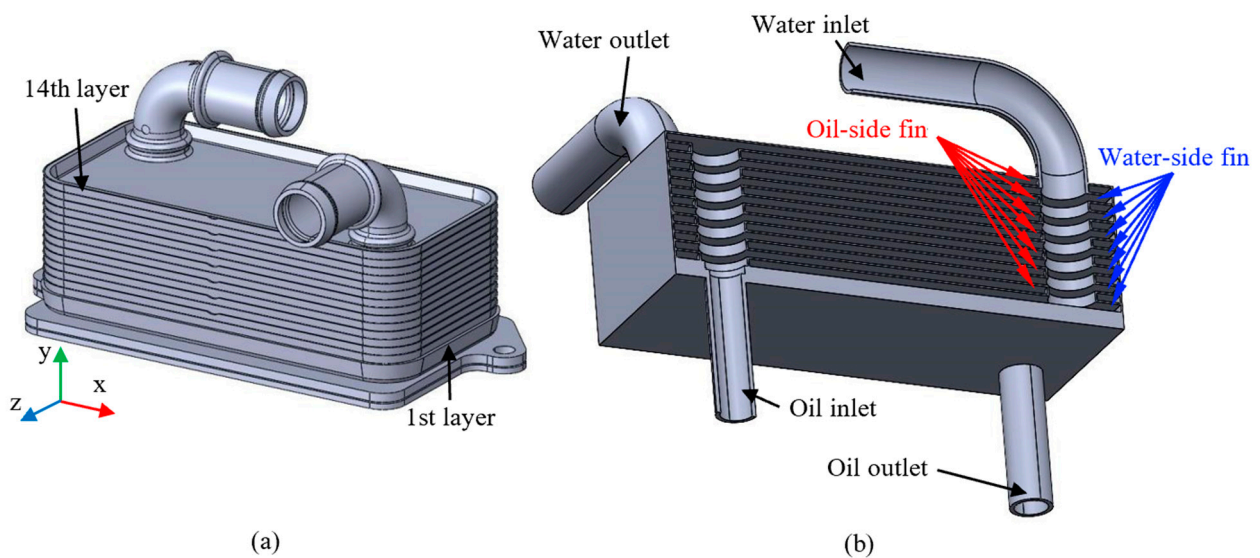

(a)   (b)

Figure 1. The heat exchangers are modeled from bottom to top as layers 1 to 14, where the odd-numbered layers are water-side fins and the even-numbered layers are oil-side fins: (**a**) Heat exchangers model, (**b**) Simplified model of heat exchangers.

Fluids on the oil side and the water side are 4109 lubrication oil and water, respectively, and their physical properties are shown in Tables 1 and 2. MUZYCHKA [24] classified the serrated fins into High Pressure Direction (HPD) type and Low Pressure Direction (LPD) type according to the different fluid flow directions inside the fins, as shown in Figure 2. The oil side and water side of the heat exchanger studied in this paper are HPD type fins, and both the fins and the heat exchanger are made of aluminum alloy with thermal conductivity $\lambda = 190$ W/(m × K).

Table 1. Oil parameters.

4109 Lube Physical Properties	Calculation Formula
Density/$\left(\text{kg} \times \text{m}^{-3}\right)$	$\rho_1 = -0.633t + 853.526$
Constant pressure heat ratio/$\left(\text{J} \times \text{kg}^{-1} \times \text{K}^{-1}\right)$	$C_{P1} = 5.556 \times 10^{-4}t^3 - 0.133t^2 + 13.492t + 1629.524$
Thermal conductivity/$\left(\text{W} \times \text{m}^{-1} \times \text{K}^{-1}\right)$	$\lambda_1 = 2.472 \times 10^{-5}t^3 - 0.00628t^2 + 0.330t + 133.610$
Dynamic viscosity/$(\text{Pa} \times \text{s})$	$\mu_1 = -4.785 \times 10^{-8}t^3 + 1.455 \times 10^{-5}t^2 - 0.00155t + 0.0618$

Table 2. Water parameters.

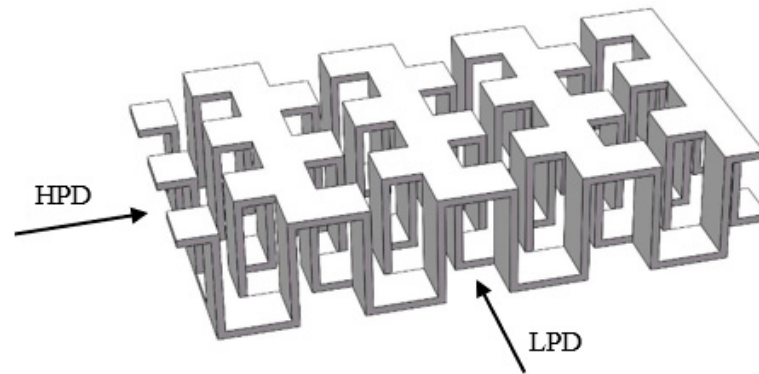| Water Physical Properties	Calculation Formula
Density/$(\mathrm{kg} \times \mathrm{m}^{-3})$	$\rho_2 = 1000.7 - 0.0852t - 0.0034t^2$
Constant pressure heat ratio/$(\mathrm{J} \times \mathrm{kg}^{-1} \times \mathrm{K}^{-1})$	$C_{P2} = 4184.4 - 0.6964t + 1.036 \times 10^{-2}t^2$
Thermal conductivity/$(\mathrm{W} \times \mathrm{m}^{-1} \times \mathrm{K}^{-1})$	$\lambda_2 = 0.5980 + 1.373 \times 10^{-3}t - 5.333 \times 10^{-6}t^2$
Dynamic viscosity/$(\mathrm{Pa} \times \mathrm{s})$	$\mu_1 = 0.00178 - 4.607 \times 10^{-5}t + 5.285 \times 10^{-7} - 2.156 \times 10^{-9}$

Figure 2. Fin model.

The heat exchanger can increase the heat transfer quantity by increasing the flow rate during operation, but this approach inevitably leads to an increase in the pressure drop on the oil and water sides, thus increasing the cost of the oil pump and motors. In turn, reducing the pressure drop makes the heat transfer quantity drop, leading to a decrease in heat exchanger performance. Therefore, finding the optimal inlet flow rate is essential to fully utilize the performance of the heat exchanger. There have been numerous studies showing that the geometric parameters of the fins have a significant effect on the pressure drop and heat transfer, and that finding the optimal fin angle can also fully improve the heat exchanger performance. In this study, the heat exchanger is simulated with different inlet flow rates and fins of different angles. The inlet flow rates are the oil flow rate and the water flow rate. The fin angles are shown in Figure 3, where the solid line is for 90° fins and the dashed line is for 75° fins. The fin angles range from 30° to 90°, with a set of parameters taken at 15° intervals, for a total of 5 different fin angles.
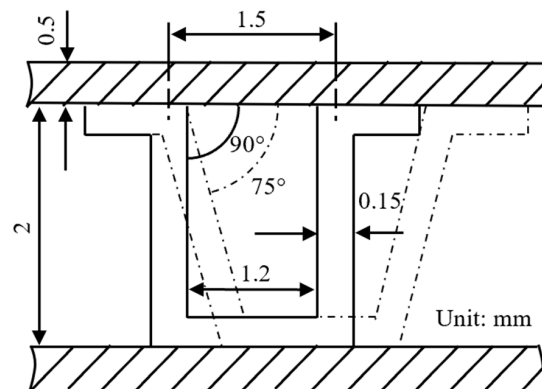

Figure 3. The solid line is 90-degree fin, and the dashed line is 75-degree fin.

2.2. Porous Media Model

Due to the difference of several orders of magnitude between the geometric size of the fin and the overall size of the heat exchanger, if the overall flow and heat transfer

performance of the heat exchanger is to be calculated by numerical simulation on the premise of retaining the geometric shape of the whole fin, the number of meshes will exceed 1 billion. The existing computer is difficult to meet its huge computational volume. Therefore, in this study, the porous media model is used to replace the fin region with complex and dense structure.

Patankar et al. [15] first to applied the porous media model to the overall study of heat exchangers, where the fluid heat transfer and pressure drop through the fin region were approximated with the porous effect. This approximation sacrifices the details of the flow heat transfer in the simplified region, but allows the overall performance of the heat exchanger to be studied by virtue of a smaller computational volume. The porous media distribution resistance model is [16,25]:

$$S_i = -\Delta P_i = -(a_1 u_i + a_2 |u_i| u_i) \tag{1}$$

where S_i is the i-directional (x, y, z) momentum source term, ΔP_i is the fluid pressure drop per unit length, a_1, a_2 are constants, u_i is the i-directional fluid rate, and the resistance of the fins to the fluid is expressed on the momentum equation through the source term S_i. The resistance of the fins in each direction is not uniform and all are calculated using this model. Ultimately, the anisotropic porous media model is obtained.

In the working process of heat exchanger, there is a certain temperature difference between the fluid and the solid. Therefore, the porous medium model is a non-thermal equilibrium model, and this model uses different energy conservation equations for the fluid and the solid, respectively [26], where the fluid energy equation is:

$$\gamma \frac{\partial(c_f \rho_f T_f)}{\partial t} + \nabla \cdot \left(\rho_f V_f c_f T_f \right) = \nabla \cdot \left(k_{f,eff} \nabla T_f \right) + h_{sf} A_{sf} \left(T_s - T_f \right) \tag{2}$$

where γ is the porosity of the medium, c_f is the fluid specific heat capacity at constant pressure, ρ_f is the fluid density, T_f is the fluid temperature, V_f is the fluid rate, $k_{f,eff}$ is the fluid equivalent thermal conductivity, h_{sf} is the fluid-solid heat transfer coefficient, A_{sf} is the specific surface area, and T_s is the solid temperature. The solid energy equation is:

$$(1 - \gamma)\rho_s c_s \frac{\partial(T_s)}{\partial t} = \nabla \cdot \left(k_{s,eff} \nabla T_s \right) - h_{sf} A_{sf} \left(T_s - T_f \right) \tag{3}$$

where c_s is the constant pressure specific heat capacity of the solid, ρ_s is the density of the solid, $k_{s,eff}$ is the equivalent thermal conductivity of the solid.

Using Equation (1), the inertia resistance coefficient and viscous resistance coefficient of the corresponding porous media with different angle fins can be calculated by the contrast coefficient method. The fins with different angles are expressed by different parameters of the porous media model, and the calculated results are shown by Table 3.

Table 3. Porous media parameters at different fin angles.

Fin Angle (Degree)	Direction	Oil-Side		Water-Side	
		Inertia Resistance Coefficient	Viscous Resistance Coefficient	Inertia Resistance Coefficient	Viscous Resistance Coefficient
30	x	654.11	13,010,483.22	573.70	22,446,726.77
	y	154.93	8,314,874.37	100.33	13,005,541.29
	z	2107.09	15,091,688.08	2760.85	9,890,534.41
45	x	1694.94	24,366,827.96	2032.31	32,193,073.73
	y	180.32	9,280,325.13	98.58	15,460,070.31
	z	958.91	13,388,172.00	1297.63	15,674,043.86

Table 3. *Cont.*

Fin Angle (Degree)	Direction	Oil-Side		Water-Side	
		Inertia Resistance Coefficient	Viscous Resistance Coefficient	Inertia Resistance Coefficient	Viscous Resistance Coefficient
60	x	3085.18	27,150,232.23	3696.54	50,883,478.55
	y	211.48	11,140,364.43	111.96	17,094,499.37
	z	489.32	13,550,495.64	611.80	18,247,912.26
75	x	4932.33	34,927,706.55	5421.13	111,562,991.10
	y	260.39	14,989,419.77	142.80	21,038,545.35
	z	260.68	15,760,390.93	251.51	22,156,993.76
90	x	8109.04	64,959,109.79	9404.43	145,279,021.40
	y	431.28	22,517,311.17	227.92	32,326,301.05
	z	231.38	23,986,847.43	150.94	30,901,507.98

2.3. Governing Equation

The CFD solution of the heat exchanger model is performed using fluid-solid coupling based on the commercial software Fluent. To simplify the calculations, the following assumptions are made [27,28]:

(1) Since the thickness of the baffle in the heat exchanger is only 0.5 mm, the temperature difference in the baffle thickness direction is neglected.
(2) Ignore the influence of radiation heat transfer.
(3) No sliding at the fluid-solid interface.
(4) The system is insulated.

Based on the above assumptions, the governing equations for plate-fin heat exchangers are Mass conservation equations:

$$\frac{\partial}{\partial x_i}(u_i) = 0 \tag{4}$$

Momentum conservation equation:

$$\frac{\partial}{\partial x_i}(\rho u_i u_k) = \frac{\partial}{\partial x_i}\left(\mu \frac{\partial u_k}{\partial x_i}\right) - \frac{\partial P}{\partial x_k} \tag{5}$$

Energy conservation equation:

$$\frac{\partial(\rho u_i u_j)}{\partial x_j} = -\frac{\partial P}{\partial x_i} + \frac{\partial}{\partial x_j}\left(\mu \frac{\partial u_i}{\partial x_j} - \rho u_i u_j\right) \tag{6}$$

where x is the direction, u is the velocity of the fluid, ρ is the density of the fluid, μ is the dynamic viscosity of the fluid, and P is the pressure.

2.4. Boundary Conditions

In addition to the solid domain of the model, two fluid domains, oil-side, and water-side, are defined in Fluent software for the heat exchanger model. All three simulation domains are meshed using tetrahedral unstructured meshes. A shear stress transport k-ω turbulence model (SST k-ω) and standard wall functions are used for numerical simulations, and velocity inlet and pressure outlet boundary conditions are used for both the oil and water sides. The heat exchanger walls are all set as wall boundary conditions with thermal conductivity and the other external walls are set as insulation walls. In order to obtain the best performance of the heat exchanger, 9 numerical simulation test groups (5 numerical simulation cases per group, 45 numerical simulation cases in total) are designed with oil flow rate, water flow rate, and the fin angle as input parameters, as shown in Table 4. Among them, the inlet flow rate covers the operating range of the heat exchanger, the oil inlet temperature is constant at 100 °C, and the water inlet temperature is constant at 65 °C.

Table 4. Simulated cases of the present study.

Simulation Group No.	Oil-Side Flow Rate (L/min)	Water-Side Flow Rate (L/min)	Fin Angle (Degree)
A	5	5	
B	5	10	
C	5	15	
D	10	5	
E	10	10	30, 45, 60, 75, 90
F	10	15	
G	15	5	
H	15	10	
I	15	15	

2.5. Verification of Simulation Results

Calibration calculations of heat exchangers can be well performed using the η-NTU method, and the accuracy of the η-NTU method has long been demonstrated by a large number of scholars [29,30]. However, the calculation process of the η-NTU method is very tedious. Therefore, in this study, when using the η-NTU method to verify the numerical simulation results, we only take the fin angle 90° as an example to verify the A, E, and I groups in Table 4. The three numerical simulation cases are renamed as I, II, and III, as shown by Table 5.

As shown in Figure 4, the average error of heat transfer quantity is 4.61% and the average error of oil outlet temperature is only 0.96%. The average error of oil pressure drop is 4.64%, and the average error of water pressure drop is 4.66%. The results show that the flow-solid coupling model established in this paper has good accuracy.
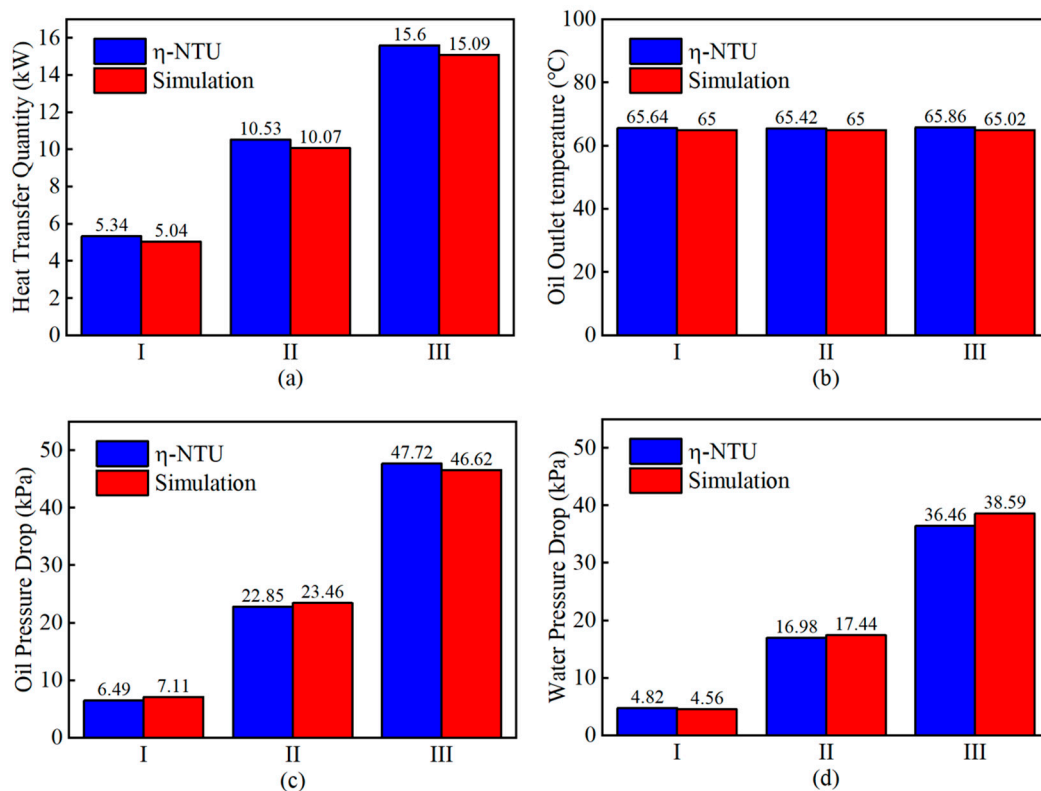

Figure 4. Comparison of η-NTU calculation results and simulation results: (**a**) Heat transfer quantity, (**b**) Oil outlet temperature, (**c**) Oil pressure drop, (**d**) Water pressure drop.

Table 5. Three simulated cases for validation via η-NTU.

Simulation Serial No.	Oil-Side Flow Rate (L/min)	Water-Side Flow Rate (L/min)	Fin Angle (Degree)
I	5	5	90
II	10	10	90
III	15	15	90

3. Multi-Objective Optimization

3.1. Optimization Objectives and Optimization Parameters

Heat exchanger as one of the heat dissipation components of the engine, heat transfer quantity and pressure drop are important indicators to evaluate its performance. The greater the heat transfer quantity, the better, and the smaller the pressure drops, the better. However, heat transfer quantity and pressure drop are contradictory to each other, and increasing heat transfer will inevitably lead to the increase of pressure drop, and vice versa. At the same time, during the operation of the heat exchanger, the closer the oil outlet temperature is to the water inlet temperature, the better. According to the simulation and η-NTU calculation results, the oil pressure drop is much larger than the water pressure drop during the working process of the heat exchanger. Therefore, the optimization objectives established in this paper are heat transfer quantity, oil pressure drop, and oil outlet temperature.

The law of heat transfer and flow in the heat exchanger is complex, and selecting the appropriate inlet flow rate on the oil side and the water side can give full play to the performance of the heat exchanger. In addition, changing the key parameters of the fins can effectively adjust the pressure drop and heat transfer quantity of the heat exchanger. There are many key geometric parameters of fins, but studies on fin angles are rare. Therefore, the optimized parameters for this study are determined as fin angle, oil flow rate, and water flow rate.

3.2. SVR Regression Model

After the data of 45 test cases are obtained by numerical simulation, it is necessary to fit them to obtain the regression models of heat transfer quantity, oil pressure drop and oil outlet temperature with respect to fin angle, oil flow rate and water flow rate. These regression models will be used as objective functions of multi-objective optimization.

Support vector regression (SVR) is an extension of support vector machine (SVM), which is widely used for regression of engineering problems. The given data set is set as $D = \{(x_1, y_1), (x_2, y_2), ..., (x_n, y_n)\}$, where $x_i \in R_n$ is the vector of input variables and $y_i \in R_n$ is the corresponding scalar output (target) value. The target of SVR is to minimize the "distance" to the farthest sample point of the fitted hyperplane, so as to accurately predict the target $\{y_i\}$ corresponding to a set of input samples $\{x_i\}$.

SVR creates a "spacing band" on both sides of the hyperplane with a spacing of ε (tolerance bias), and does not calculate the loss for all samples that fall into the spacing band. For the linear problem, SVR constructs the following linear model [31,32]:

$$f(x_i) = \omega x_i + b \tag{7}$$

Thus, its optimization objective is:

$$\begin{cases} \min \frac{1}{2}||\omega||^2 \\ s.t. |y_i - (\omega x_i + b)| \leq \varepsilon, \ \forall i \end{cases} \tag{8}$$

SVR allows for the presence of samples outside the spacing band, but the losses should be as small as possible so that the optimization objective of SVR can be formalized as:

$$\min \frac{1}{2}||\omega||^2 + C \sum_{i=1}^{m} L_c(f(x_i), y_i) \tag{9}$$

where $C \sum_{i=1}^{m} L_c(f(x_i), y_i)$ is the empirical error term of SVR, consisting of a loss function $L_C(f(x_i), y_i)$ and a factor C. The loss function is expressed as:

$$L_C(f(x_i), y_i) = \begin{cases} 0, & |y_i - f(x_i)| \le \varepsilon \\ |y_i - f(x_i)| - \varepsilon, & |y_i - f(x_i)| > \varepsilon \end{cases} \tag{10}$$

and the factor C represents the weights. To explain the error beyond the limit ε, the relaxation variables ξ and ξ^* are introduced. At this point, all sample data meet the condition:

$$|y_i - (\omega x_i + b)| \le \varepsilon + \xi, \ \forall i \tag{11}$$

The relaxation variable transforms the SVR problem into a dual optimization problem, and its optimization objectives are:

$$\begin{cases} \min_{\omega, b, \xi_i, \xi_i^*} \frac{1}{2} ||\omega||^2 + C \sum_{i=1}^{m} (\xi_i, \ \xi_i^*) \\ s.t. y_i - f(x_i) \le \varepsilon + \xi_i \\ \quad f(x_i) - y_i \le \varepsilon + \xi_i^* \\ \quad \xi_i, \xi_i^* \ge 0, i = 1, 2, \dots m \end{cases} \tag{12}$$

The optimization problem with constraints can be transformed into an unconstrained optimization problem by Lagrange multiplier method. With the introduction of Lagrange multipliers α_i and α_i^*, the linear model can be rewritten as:

$$f(x) = \omega x + b = \sum_{i=1}^{m} (\alpha_i - \alpha_i^*) x_i^T x + b \tag{13}$$

For nonlinear problems, the nonlinear problem can be mapped to a linear problem by boosting the sample dimension. However, when the data dimension itself is large, boosting can make the computational effort increase dramatically. To overcome the contradiction between high-dimensional feature space and computational complexity, SVR will define appropriate kernel functions [33]. With the help of kernel functions, the results of the inner product of samples in the high-dimensional space can be computed directly in the low-dimensional space, thus greatly reducing the computational effort. The choice of kernel function requires that Mercer's theorem is satisfied, i.e., the kernel function is semi-positive definite for any Gram matrix in the sample space [34]. The Gaussian radial basis function (RBF), also called Radial Basis Function, can map the data to infinite dimensions with the expression [35,36]:

$$K(x_i, x_j) = \phi(x_i)^T \phi(x_j) = \exp\left(-\frac{1}{2\sigma^2} ||x_i - x_j||^2\right) = \exp\left(-\gamma ||x_i - x_j||^2\right) \tag{14}$$

where $i, j = 1 \dots m$, σ is the width of the RBF. After the SVR is mapped into the kernel function, its model can be rewritten as:

$$f(x) = \omega \phi(x) + b = \sum_{i=1}^{m} (\alpha_i - \alpha_i^*) K(x_i, x_j) + b \tag{15}$$

where $\phi(x)$ is the mapping function that maps x to a higher dimensional space.

Since the RBF kernel has good universality and depends on only one parameter σ, the RBF kernel function is chosen to build the SVR regression model in this study. Meanwhile, the data of 45 simulation cases are fitted with the fin angle, oil flow rate, and water flow rate as input parameters, and the regression models of heat transfer quantity, oil pressure drop, and oil outlet temperature are finally obtained. These models will be used as the objective function for multi-objective optimization.

3.3. Multi-Objective Optimization Based on NSGA-II Algorithm

There are two main types of multi-objective optimization algorithms: ordinary gradient methods and gradient-free direct methods. The first type of method relies on the quality of the initial guess, which is easy to fall into local extremes and is only applicable to continuous smooth functions. The gradient-free direct method is more suitable for the study of nonlinear phenomena. Among them, genetic algorithms are the most widely used [37,38]. Such algorithms are insensitive to the discontinuity of the objective function, do not get trapped in local optima, and are suitable for parallel processing.

NSGA-II is a kind of genetic algorithm that can efficiently order the nondominated solutions while providing a set of Pareto optimal solutions well distributed along the Pareto frontier and considering an elite strategy of accelerating convergence [39]. The algorithm is widely used to minimize or maximize two or more objective functions under given constraints and boundary conditions. The result of its optimization represents the set of solutions with the best compromise between the objective functions.

NSGA-II generates a random population in the initial state, and then the population individuals undergo crossover (parents produce offspring) and mutation (small random changes in offspring). The algorithm then sorts individuals based on non-dominance rank and crowding degree, and selects higher quality individuals to form the next generation. The population is driven towards the optimal Pareto frontier while maintaining the diversity of the population [40]. The algorithm runs until a predefined number of generations is reached.

In this study, NSGA-II was used to optimize three conflicting objective functions (heat transfer quantity, oil pressure drop, oil outlet temperature). The population size, crossover probability, mutation probability, and maximum number of generations are set to 2000, 0.9, 0.2, and 5000, respectively. The boundary conditions are:

(1) $30° \leq$ Fin angle $\leq 90°$;
(2) L/min $\leq$ Oil flow rate ≤ 15 L/min;
(3) L/min $\leq$ Water flow rate ≤ 15 L/min.

3.4. Multi-Objective Decision Making Based on TOPSIS Algorithm

The optimal solution set with 2000 solutions is eventually obtained using NSGA-II, and the multi-objective decision making method can prefer the optimal solution from it. TOPSIS is one of the most commonly used multi-objective decision making methods for selecting the best compromise solution between the incommensurable and conflicting objective functions [22]. The optimal solution based on TOPSIS decision making is closest to the positive ideal solution and farthest from the negative ideal solution. The steps of TOPSIS multi-objective decision making are as follows:

Step 1: Create a decision matrix $(a_{ij})m \times n$, where m is the decision point and n is the number of objective functions.

Step 2: Normalize the decision matrix using the Euclidean method:

$$x_{ij} = \frac{a_{ij}}{\sqrt{\sum_{j=1}^{m} a_{ij}^2}}, \ i = 1, 2, \cdots, m; j = 1, 2, \cdots, n \tag{16}$$

Step 3: Develop a weighted normalized decision matrix:

$$X_{ij} = x_{ij} \times w_j, \ i = 1, 2, \cdots, m; j = 1, 2, \cdots, n \tag{17}$$

where $\sum_{j=1}^{n} w_j = 1$.

Step 4: Determine positive ideal solutions (X^+) and negative ideal solutions (X^-):

$$X^+ = \left[\left(\max_i X_{ij} \middle| j \in J_+ \right), \left(\min_i X_{ij} \middle| j \in J_- \right) \middle| i = 1, 2, \cdots, m \right] = \left\{ X_1^+, X_2^+, \ldots, X_n^+ \right\} \tag{18}$$

$$X^- = \left[\left(\min_i X_{ij}\middle| j \in J_+\right), \left(\max_i X_{ij}\middle| j \in J_-\right)\middle| i = 1, 2, \cdots, m\right] = \left\{X_1^-, X_2^-, \ldots, X_n^-\right\} \tag{19}$$

where J_+ is the indicator of positive standard, J_- is the indicator of negative standard, and X_n^+ and X_n^- are the maximum and minimum values of each column, respectively.

Step 5: Calculate the distance of each objective alternative from the positive ideal solution and the negative ideal solution:

$$D_i^+ = \sqrt{\sum_{j=1}^{n}\left(X_{ij} - X_j^+\right)^2}, \, i = 1, 2, \ldots, m \tag{20}$$

$$D_i^- = \sqrt{\sum_{j=1}^{n}\left(X_{ij} - X_j^-\right)^2}, \, i = 1, 2, \ldots, m \tag{21}$$

Step 6: Calculate the relative proximity of each objective alternative to the ideal state:

$$C_l^* = \frac{D_i^-}{D_i^- + D_i^+}, \, i = 1, 2, \ldots, m \tag{22}$$

The solution of TOPSIS is the point with the largest value of C_l^* on the Pareto optimal solution set. If the solution of TOPSIS is not reasonable, the weights (w_j) of the objective function can be reassigned and the results are recalculated. In this study, the weights of all optimization objectives are set to be equal, i.e., the weights of heat transfer quantity, oil pressure drop, and oil outlet temperature are all 1/3. The TOPSIS algorithm is used to make decisions among 2000 optimal solutions, and the optimal result is preferentially selected.

In summary, the overall optimization process for the plate-fin heat exchanger is shown in Figure 5. Firstly, the data of numerical simulation was obtained using the fluid-solid coupling model of the plate-fin heat exchanger, and then the regression models of heat transfer quantity, oil pressure drop, and oil outlet temperature with respect to the fin angle, oil flow rate, and water flow rate are obtained by SVR. Additionally, these regression models are used as the objective function for multi-objective optimization. NSGA-II is utilized to optimize on the objective function to obtain the Pareto optimal solution set. Finally, TOPSIS is applied to decide the optimal solution in the solution set.
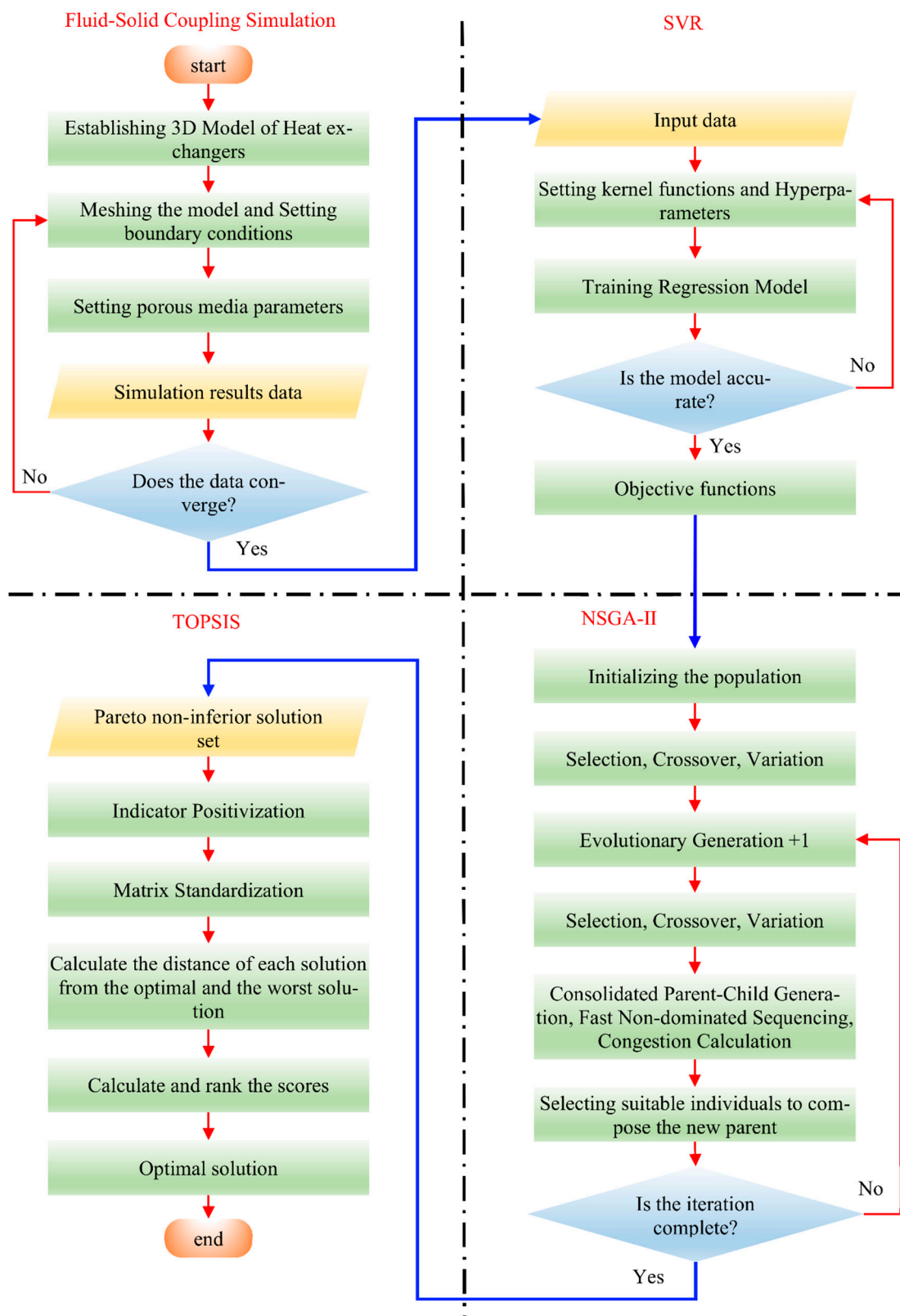
Figure 5. Flow chart of fluid-solid coupling simulation, SVR prediction model, and multi-objective optimization.

4. Results and Discussion

4.1. Simulation Results

Figure 6 shows the results of the 9 simulation groups listed in Table 4. Among them, the oil flow rates for groups A, B, and C were 5 L/min, and the water flow rates were 5, 10, and 15 L/min, respectively. In groups D, E, and F, the oil flow rates were 10 L/min, and the water flow rates were 5, 10, and 15 L/min, respectively. Groups G, H, and I had an oil flow rate of 15 L/min, and water flow rates of 5, 10, and 15 L/min, respectively. The range of 5–15L/min covers the working range of the flow rate for the plate-fin heat exchanger used in this study.
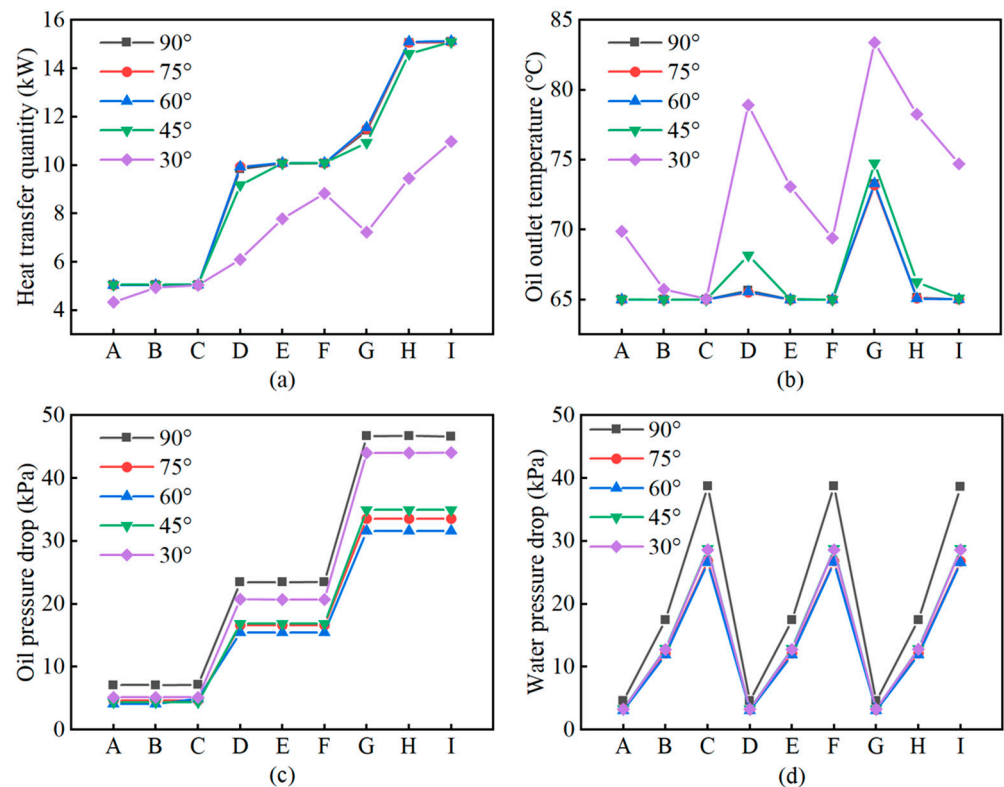

Figure 6. Simulation result, inlet flow on oil and water sides corresponding to simulation group numbers A to I is listed in Table 3: (**a**) heat transfer quantity of the heat exchangers, (**b**) oil outlet temperature, (**c**) oil pressure drop, (**d**) water pressure drop.

For heat exchangers, the higher the heat transfer quantity, the better the performance of the heat exchanger. The simulation results of heat transfer quantity for the heat exchanger are shown in Figure 6a. As the fin angle decreased, the amount of heat transfer quantity decreased. When the fin angle was reduced from 90° to 60°, the heat transfer quantity is almost unchanged for the same flow rate. When the fin angle was reduced to 45°, the heat transfer quantity decreased compared to the large angle fins at the same flow rate. When the fin angle was further reduced to 30°, the heat transfer quantity decreased significantly. Overall, the heat transfer quantity showed a rising trend with the increase of the flow rate on the oil side and water side. When the oil flow rate was less than or equal to 10 L/min, it is obvious that the oil flow rate had more influence on the heat transfer quantity than the water flow rate. The heat transfer rate showed a significant increase with the increase of the oil flow rate (group C–D). However, when the oil flow rate increased to 15 L/min, the increase of the water flow rate also caused a dramatic change of heat transfer quantity (Group G–I). That is, when the oil flow rate was less than or equal to 10 L/min, the change of heat transfer mainly depended on the oil flow rate. Additionally, when the oil flow rate was more than 10 L/min, the change of heat transfer mainly depended on the flow rate on the water side. Additionally, the larger the fin angle was, the more obvious this law was.

The closer the oil outlet temperature was to the water inlet temperature (65 °C), the better the performance of the heat exchanger. The simulation results of the oil outlet temperature for the heat exchanger are shown in Figure 6b. As the fin angle gradually decreased, the oil outlet temperature gradually increased at the same flow rate. When the fin angle was less than 45°, the trend of increasing oil outlet temperature would be very obvious. It is important to note that a higher heat transfer quantity did not mean a lower oil outlet temperature (groups C–D, F–G). In fact, there was no inevitable relationship between the oil outlet temperature and the heat transfer quantity, and almost the same oil-side outlet temperature may correspond to a very different heat transfer quantity (groups B, E, I).

The lower the pressure drop in the heat exchanger, the lower the cost of the oil pump and motor. The simulation results of the oil pressure drop and the water pressure drop are shown in Figure 6c, respectively. It was obvious that the flow rate is directly proportional to the pressure drop. The oil flow rate had a significant effect on the oil pressure drop, while the water flow rate had almost no effect on the oil pressure drop. The same was true for the water pressure drop, which was almost independent of the change in oil flow rate. This is because the pressure drop is not transferred between the oil and water sides like heat. At the same time, the oil pressure drop was much higher than that of the water side at the same flow rate. In addition, when the fin angle was reduced from 90° to 60°, the pressure drop decreased as the fin angle became smaller for the same flow rate. However, when the fin angle further decreased from 60° to 30°, the pressure drop increased as the fin angle became smaller. That is, the pressure drop underwent a process of becoming smaller and then larger as the fin angle decreased.

In a word, there is a contradiction among the three objective functions: heat transfer, oil pressure drop, and oil outlet temperature. The effects of fin angle, oil flow rate, and water flow rate on the objective function are interrelated.

4.2. Multi-Objective Optimization

Since the optimization direction of the objective function is not consistent, the use of multi-objective optimization algorithm can effectively obtain the optimal solution among the objective functions. However, discrete simulation results cannot be used for multi-objective optimization search, and the discrete results must be turned into objective functions. The 45 cases of simulation data of the heat exchanger are shown in Table 6, and the regression models of heat transfer quantity, oil pressure drop and oil outlet temperature with respect to fin angle, oil flow rate, and water flow rate are obtained by fitting these data with SVR.

Table 6. Simulation data.

No.	Design Variables			Objective Function		
	Fin Angle (Degree)	Oil Flow Rate (L/min)	Water Flow Rate (L/min)	Heat Transfer Quantity (kW)	Oil Pressure Drop (kPa)	Oli Outlet Temperature (°C)
1	30	5	5	5.04	7.11	65.00
2	30	5	10	5.04	7.11	65.00
3	30	5	15	5.04	7.12	65.00
4	30	10	5	9.84	23.44	65.65
5	30	10	10	10.07	23.46	65.00
6	30	10	15	10.08	23.49	65.00
7	30	15	5	11.43	46.67	73.28
8	30	15	10	15.06	46.73	65.14
9	30	15	15	15.09	46.62	65.02
10	45	5	5	5.04	4.64	65.00
11	45	5	10	5.04	4.64	65.00
12	45	5	15	5.04	4.64	65.00
13	45	10	5	9.94	16.62	65.52
14	45	10	10	10.08	16.63	65.00
15	45	10	15	10.08	16.62	65.00
16	45	15	5	11.51	33.57	73.18
17	45	15	10	15.07	33.56	65.10

Table 6. *Cont.*

No.	Design Variables			Objective Function		
	Fin Angle (Degree)	Oil Flow Rate (L/min)	Water Flow Rate (L/min)	Heat Transfer Quantity (kW)	Oil Pressure Drop (kPa)	Oli Outlet Temperature (°C)
18	45	15	15	15.10	33.55	65.01
19	60	5	5	5.04	4.13	65.00
20	60	5	10	5.04	4.13	65.00
21	60	5	15	5.05	4.92	65.00
22	60	10	5	9.93	15.46	65.56
23	60	10	10	10.09	15.46	65.00
24	60	10	15	10.09	15.45	65.00
25	60	15	5	11.55	31.59	73.29
26	60	15	10	15.10	31.60	65.07
27	60	15	15	15.12	31.60	65.00
28	75	5	5	5.05	4.40	65.00
29	75	5	10	5.05	4.39	65.00
30	75	5	15	5.05	4.39	65.00
31	75	10	5	9.18	16.85	68.16
32	75	10	10	10.08	16.85	65.03
33	75	10	15	10.09	16.85	65.00
34	75	15	5	10.93	34.94	74.75
35	75	15	10	14.60	34.94	66.25
36	75	15	15	15.09	34.95	65.10
37	90	5	5	4.34	5.16	69.88
38	90	5	10	4.94	5.15	65.72
39	90	5	15	5.04	5.16	65.06
40	90	10	5	6.10	20.73	78.91
41	90	10	10	7.78	20.71	73.07
42	90	10	15	8.83	20.70	69.41
43	90	15	5	7.23	44.03	83.39
44	90	15	10	9.45	44.02	78.26
45	90	15	15	10.98	44.05	74.70

The error of the SVR regression model regarding the 45 cases of simulation data is shown in Figure 7 and the maximum error did not exceed 2.5%. In fact, the boundary conditions of the simulation, i.e., oil flow and water flow (5–15 L/min), already covered the operating range of the heat exchanger. Therefore, the regression models did not need to predict the out-of-range data. These regression models would be used as the objective function for multi-objective optimization search.
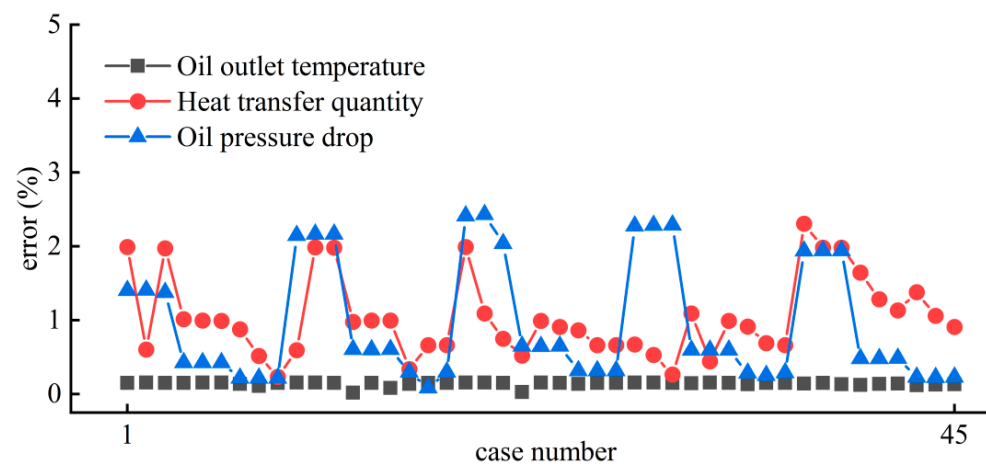

Figure 7. Percentage error of heat transfer quantity, oil pressure drop, and oil outlet temperature.

NSGA-II is a genetic algorithm that can minimize or maximize two or more objective functions under given constraints and boundary conditions. The three objective functions selected in this study were heat transfer quantity, oil pressure drop, and oil outlet temperature. In the process of heat exchanger operation, the smaller the oil pressure drop, the

smaller the oil outlet temperature, and the larger the heat transfer quantity, the better. In other words, the optimization directions of the three objective functions were not consistent. Therefore, in the process of multi-objective optimization using NSGA-II, a negative sign was added before the objective function of heat transfer quantity to unify the optimization direction of objective functions to the minimum. The set of Pareto optimal solutions obtained by NSGA-II is shown in Figure 8, which contains a total of 2000 optimal solutions.
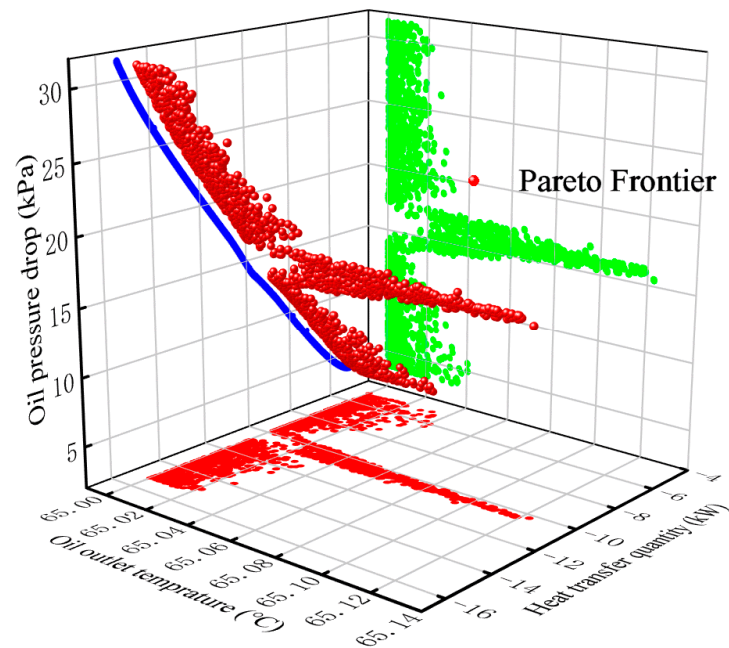

Figure 8. The distribution of Pareto optimal solutions.

After obtaining the optimal solution set, TOPSIS was used to evaluate the 2000 data comprehensively to decide the optimal solution and obtain the corresponding optimal parameters. In this study, the optimal fin angle for heat exchanger operation was 63.01°, and the optimal oil flow rate and water flow rate were 9.7 L/min and 6.45 L/min, respectively. Under these conditions, the heat transfer quantity of the heat exchanger was 9.76 kW, the oil pressure drop was 14 kPa, and the oil outlet temperature was 65 °C. The optimal parameters were brought into the simulation model and the results obtained are shown in Figure 9.
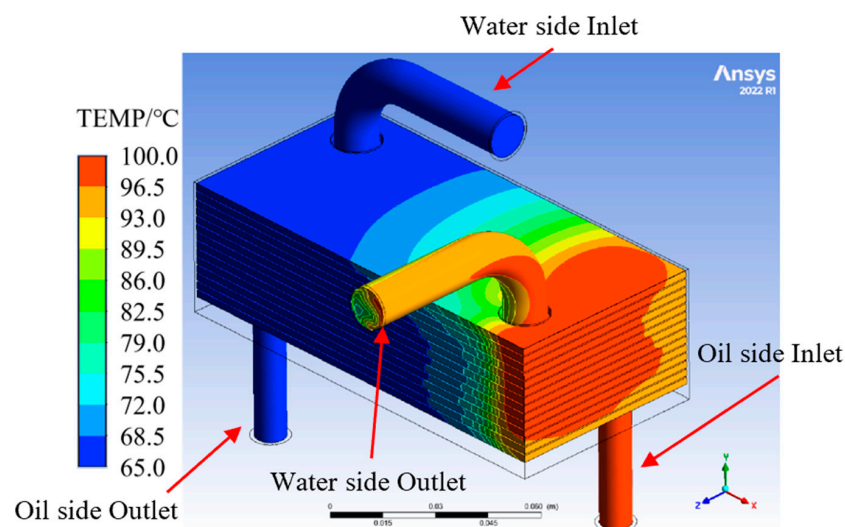

Figure 9. Simulation results of optimal parameters.

Table 7 shows the comparison between the optimal solution and the simulation results based on the optimal parameters. The errors of heat transfer quantity, oil pressure drop, and oil outlet temperature were 0.31%, 2.64%, and 0.17%, respectively. The numerical simulation results verify the correctness of the optimization results.

Table 7. Comparison of optimization results and simulation results under optimal parameters.

	Optimization Parameters			Optimization Objectives		
	Fin Angle (Degree)	Oil Flow Rate (L/min)	Water Flow Rate (L/min)	Heat Transfer Quantity (kW)	Oil Pressure Drop (kPa)	Oil Outlet Temperature (°C)
Optimization results	63.01	9.7	6.45	9.76	14	65
Simulation results	63.01	9.7	6.45	9.79	13.63	65.11
Error (%)				0.31	2.64	0.17

5. Conclusions

In order to obtain the best performance of the plate-fin heat exchanger, in this paper, the heat transfer quantity, oil pressure drop and oil outlet temperature of a plate-fin heat exchanger used in the extended-range hybrid vehicle engine were taken as the optimization objectives, and the three parameters of fin angle, oil flow rate, and water flow rate were optimized. A heat exchanger fluid-solid coupling model was established based on porous media, and the correctness of the model was verified by the η-NTU method. Based on 45 cases of simulation results, a regression model of the optimization objective was established with SVR, and then the NSGA-II algorithm was applied to obtain a Pareto solution set containing 2000 optimal solutions. Finally, the optimal solution was evaluated comprehensively by using TOPSIS. The main conclusions are summarized as follows:

(1) There is a contradiction between heat transfer quantity and pressure drop of heat exchanger, and there is no inevitable relationship between oil outlet temperature and heat transfer quantity.

(2) The heat transfer quantity of the heat exchanger is mainly influenced by the fin angle, oil flow rate, and water flow rate. The heat transfer quantity decreases as the decrease of the fin angle. When the oil flow rate is less than or equal to 10 L/min, the change of heat transfer quantity mainly depends on the oil flow rate. When the oil flow rate is greater than 10 L/min, the change of heat transfer quantity mainly depends on the water flow rate.

(3) The pressure drop in the heat exchanger is mainly influenced by the fin angle and the flow rate. As the fin angle decreases from 90° to about 60°, the pressure drop also decreases. However, as the fin angle continues to decrease, the pressure drop increases. The oil flow rate or the water flow rate does not affect the pressure drop variation on the other side.

(4) When the fin angle is 63.01°, the oil flow rate is 9.7 L/min and the water flow rate is 6.45 L/min, the heat exchanger achieves the best performance. Under this condition, the heat transfer quantity of the heat exchanger is 9.76 kW, the oil pressure drop is 14 kPa, and the oil outlet temperature is 65 °C.

Author Contributions: Conceptualization, S.L. and D.L.; methodology, S.L. and D.L.; software, S.L.; resources S.L; investigation, S.L. and Z.D.; data curation J.L. and Z.D.; writing-original draft preparation, S.L.; writing-review and editing, D.L.; visualization, S.L. and J.L.; funding acquisition, D.L. The manuscript was reviewed by all authors. All authors have read and agreed to the published version of the manuscript.

Institutional Review Board Statement: Not applicable.

Informed Consent Statement: Not applicable.

Data Availability Statement: Not applicable.

Conflicts of Interest: The authors declared that they do not have any commercial or associative interest that represents a conflict of interest in connection with the work submitted.

References

1. Ning, J.; Wang, X.; Sun, Y.; Zheng, C.; Zhang, S.; Zhao, X.; Liu, C.; Yan, W. Experimental and numerical investigation of additively manufactured novel compact plate-fin heat exchanger. *Int. J. Heat Mass Transf.* **2022**, *190*, 122818. [CrossRef]
2. Bhuiyan, A.A.; Islam, A.S. Thermal and hydraulic performance of finned-tube heat exchangers under different flow ranges: A review on modeling and experiment. *Int. J. Heat Mass Transf.* **2016**, *101*, 38–59. [CrossRef]
3. Xu, P.; Wen, J.; Zhao, X.; Hao, H.; Wang, S.; Li, Y. Numerical investigation on serrated fin of sub-atmosphere plate-fin heat exchanger used in superfluid helium system. *Cryogenics* **2021**, *119*, 103351. [CrossRef]
4. Zhang, Y.; Peng, J.; Yang, R.; Yuan, L.; Li, S. Weight and performance optimization of rectangular staggered fins heat exchangers for miniaturized hydraulic power units using genetic algorithm. *Case Stud. Therm. Eng.* **2021**, *28*, 101605. [CrossRef]
5. Peng, F.; Cui, G. Efficient simultaneous synthesis for heat exchanger network with simulated annealing algorithm. *Appl. Therm. Eng.* **2015**, *78*, 136–149. [CrossRef]
6. Ishaque, S.; Kim, M.-H. Refrigerant circuitry optimization of finned tube heat exchangers using a dual-mode intelligent search algorithm. *Appl. Therm. Eng.* **2022**, *212*, 118576. [CrossRef]
7. Lee, K.; Kim, M.; Ha, M.Y.; Min, J.K. Investigation of heat-exchanger-sizing methods using genetic, pattern search, and simulated annealing algorithms and the effect of entropy generation. *J. Mechan. Sci. Technol.* **2018**, *32*, 915–928. [CrossRef]
8. Bhutta, M.M.A.; Hayat, N.; Bashir, M.H.; Khan, A.R.; Ahmad, K.N.; Khan, S. CFD applications in various heat exchangers design: A review. *Appl. Therm. Eng.* **2012**, *32*, 1–12. [CrossRef]
9. Kritikos, K.; Albanakis, C.; Missirlis, D.; Vlahostergios, Z.; Goulas, A.; Storm, P. Investigation of the thermal efficiency of a staggered elliptic-tube heat exchanger for aeroengine applications. *Appl. Therm. Eng.* **2010**, *30*, 134–142. [CrossRef]
10. Tiwari, A.K.; Ghosh, P.; Sarkar, J.; Dahiya, H.; Parekh, J. Numerical investigation of heat transfer and fluid flow in plate heat exchanger using nanofluids. *Int. J. Therm. Sci.* **2014**, *85*, 93–103. [CrossRef]
11. Wang, J.; Bian, H.; Cao, X.; Ding, M. Numerical performance analysis of a novel shell-and-tube oil cooler with wire-wound and crescent baffles. *Appl. Therm. Eng.* **2021**, *184*, 116298. [CrossRef]
12. Li, W.; Paul, M.; Siviter, J.; Montecucco, A.; Knox, A.; Sweet, T.; Min, G.; Baig, H.; Mallick, T.; Han, G. Thermal performance of two heat exchangers for thermoelectric generators. *Case Stud. Therm. Eng.* **2016**, *8*, 164–175. [CrossRef]
13. Li, J.; Peng, H.; Ling, X. Numerical study and experimental verification of transverse direction type serrated fins and field synergy principle analysis. *Appl. Therm. Eng.* **2013**, *54*, 328–335. [CrossRef]
14. Kim, M.; Ha, M.Y.; Min, J.K. A numerical study on the aero-thermal performance of a slanted-pin-fin cooler under a high-speed-bypass condition. *Int. J. Heat Mass Transf.* **2018**, *119*, 791–812. [CrossRef]
15. Patankar, S.; Spalding, D. Computer analysis of the three-dimensional flow and heat transfer in a steam generator. In *Numerical Prediction of Flow, Heat Transfer, Turbulence and Combustion*; Elsevier: Amsterdam, The Netherlands, 1983; pp. 293–298. [CrossRef]
16. Zhang, Q.; Qin, S.; Ma, R. Simulation and experimental investigation of the wavy fin-and-tube intercooler. *Case Stud. Therm. Eng.* **2016**, *8*, 32–40. [CrossRef]
17. Esfe, M.H.; Mahian, O.; Hajmohammad, M.H.; Wongwises, S. Design of a heat exchanger working with organic nanofluids using multi-objective particle swarm optimization algorithm and response surface method. *Int. J. Heat Mass Transf.* **2018**, *119*, 922–930. [CrossRef]
18. Guo, K.; Zhang, N.; Smith, R. Design optimisation of multi-stream plate fin heat exchangers with multiple fin types. *Appl. Therm. Eng.* **2018**, *131*, 30–40. [CrossRef]
19. Hadidi, A. A robust approach for optimal design of plate fin heat exchangers using biogeography based optimization (BBO) algorithm. *Appl. Energy* **2015**, *150*, 196–210. [CrossRef]
20. Aminmahalati, A.; Fazlali, A.; Safikhani, H. Multi-objective optimization of CO boiler combustion chamber in the RFCC unit using NSGA II algorithm. *Energy* **2021**, *221*, 119859. [CrossRef]
21. Li, J.; Zuo, W.; Jiaqiang, E.; Zhang, Y.; Li, Q.; Sun, K.; Zhou, K.; Zhang, G. Multi-objective optimization of mini U-channel cold plate with SiO2 nanofluid by RSM and NSGA-II. *Energy* **2022**, *242*, 123039. [CrossRef]
22. Çelikbilek, Y.; Tüysüz, F. An in-depth review of theory of the TOPSIS method: An experimental analysis. *J. Manage. Analyt.* **2020**, *7*, 281–300. [CrossRef]
23. Yusuf, A.; Bayhan, N.; Tiryaki, H.; Hamawandi, B.; Toprak, M.S.; Ballikaya, S. Multi-objective optimization of concentrated Photovoltaic-Thermoelectric hybrid system via non-dominated sorting genetic algorithm (NSGA II). *Energy Convers. Manage.* **2021**, *236*, 114065. [CrossRef]
24. Muzychka, Y.S.; Yovanovich, M.M. Modeling the f and j Characteristics for Transverse Flow Through an Offset Strip Fin at Low Reynolds Number. *Heat Transf.* **1999**, *1*, 79–90. [CrossRef]
25. Huang, Y.; Liu, Z.; Lu, G.; Yu, X. Multi-scale thermal analysis approach for the typical heat exchanger in automotive cooling systems. *Int. Communicat. Heat Mass Transf.* **2014**, *59*, 75–87. [CrossRef]

26. Shivakumara, I.; Ravisha, M.; Ng, C.-O.; Varun, V. A thermal non-equilibrium model with Cattaneo effect for convection in a Brinkman porous layer. *Int. J. Non-Linear Mechan.* **2015**, *71*, 39–47. [CrossRef]

27. Zhang, J.-F.; He, Y.-L.; Tao, W.-Q. 3D numerical simulation on shell-and-tube heat exchangers with middle-overlapped helical baffles and continuous baffles–Part I: Numerical model and results of whole heat exchanger with middle-overlapped helical baffles. *Int. J. Heat Mass Transf.* **2009**, *52*, 5371–5380. [CrossRef]

28. Gu, Y.; Liu, X.; Liu, W.; Liu, Y.; Zhai, X.; Xuan, Y.; Peng, T.; Jiang, W. Research on heat transfer and pressure drop performance of plain plate fin-and-tube oil cooler. *Chem. Eng. Process. Process Intensificat.* **2020**, *158*, 108187. [CrossRef]

29. Torii, K.; Kwak, K.; Nishino, K. Heat transfer enhancement accompanying pressure-loss reduction with winglet-type vortex generators for fin-tube heat exchangers. *Int. J. Heat Mass Transf.* **2002**, *45*, 3795–3801. [CrossRef]

30. Xu, X.; Zhang, X.; Ke, P.; Wang, C.; Yang, H.; Yang, C. Study on the heat transfer characteristic of compact heat exchanger based on experimental data. *Proced. Eng.* **2015**, *121*, 293–299. [CrossRef]

31. Ahmad, M.S.; Adnan, S.M.; Zaidi, S.; Bhargava, P. A novel support vector regression (SVR) model for the prediction of splice strength of the unconfined beam specimens. *Construct. Build. Mater.* **2020**, *248*, 118475. [CrossRef]

32. Panahi, M.; Sadhasivam, N.; Pourghasemi, H.R.; Rezaie, F.; Lee, S. Spatial prediction of groundwater potential mapping based on convolutional neural network (CNN) and support vector regression (SVR). *J. Hydrol.* **2020**, *588*, 125033. [CrossRef]

33. Brereton, R.G.; Lloyd, G.R. Support vector machines for classification and regression. *Analyst* **2010**, *135*, 230–267. [CrossRef] [PubMed]

34. Pan, Y.; Jiang, J.; Wang, R.; Cao, H.; Cui, Y. A novel QSPR model for prediction of lower flammability limits of organic compounds based on support vector machine. *J. Hazard. Mater.* **2009**, *168*, 962–969. [CrossRef] [PubMed]

35. Liu, Y.; Wang, L.; Gu, K. A support vector regression (SVR)-based method for dynamic load identification using heterogeneous responses under interval uncertainties. *Appl. Soft Comput.* **2021**, *110*, 107599. [CrossRef]

36. Smola, A.J.; Schölkopf, B. A tutorial on support vector regression. *Stat. Comput.* **2004**, *14*, 199–222. [CrossRef]

37. Wang, Z.; Sobey, A. A comparative review between Genetic Algorithm use in composite optimisation and the state-of-the-art in evolutionary computation. *Compos. Struct.* **2020**, *233*, 111739. [CrossRef]

38. Gunantara, N. A review of multi-objective optimization: Methods and its applications. *Cogent Eng.* **2018**, *5*, 1502242. [CrossRef]

39. Bre, F.; Fachinotti, V.D. A computational multi-objective optimization method to improve energy efficiency and thermal comfort in dwellings. *Energy Build.* **2017**, *154*, 283–294. [CrossRef]

40. Evins, R.; Pointer, P.; Vaidyanathan, R.; Burgess, S. A case study exploring regulated energy use in domestic buildings using design-of-experiments and multi-objective optimisation. *Build. Environ.* **2012**, *54*, 126–136. [CrossRef]